DOI: 10.1002/ejic.200800095

Hollow MgO Nanotube Arrays by Using ZnO Nanorods as Templates

Hong-Bing Lu,[a] Lei Liao,[a] Hua Li,[b] Duo-Fa Wang,[a] Yu Tian,[a] Jin-Chai Li,*[a] Qiang Fu,[a] Ben-Peng Zhu,[a] and Yun Wu[a]

Keywords: MgO / Nanotubes / Chemical reactions / Template synthesis / Optical properties

A newly developed solid–gas chemical reaction route has been demonstrated to fabricate MgO nanotube arrays by using prefabricated ZnO nanorods as templates. The formation process involves the Kirkendall effect, in which the outdiffusion of the ZnO core material through the MgO shells is faster than the in-diffusion of the vapor-phase Mg atoms, resulting in the formation of Kirkendall voids, which eventually induces hollow MgO nanotubes. The dimensions and sizes of the obtained MgO nanotubes can be controlled by employing suitable ZnO templates. Other types of complex hollow MgO architectures with different aspect ratios can be further manipulated and fabricated by this method, depending on the morphologies of the starting ZnO nanostructures used as templates. These hollow MgO architectures with high surface-to-volume ratios may have promising applications in catalysis, drug delivery, nano-optics, nanoreactors, and active material encapsulation.

Introduction

Recent interest in the nanostructures has boosted the design of nanoscale materials with specific morphologies for novel device applications, since it is known that physical and chemical properties of materials are strongly influenced by their size and shape.[1–3] In comparison with other structures, hollow nanostructures exhibit stronger or novel functionalities due to their higher surface area and their capability of forming composite structures by embedding specific particles in their interiors, and they thus may find potential applications in a wide range of areas, including catalysis, drug delivery, storage and release systems, bioencapsulation, nanoreactors, and templates for functional architectural composite materials.[4–6] Hollow structures can be prepared by a number of methods, including the hydrothermal approach,[7] emulsion/water extraction techniques,[8] thermal evaporation,[9–11] or the template method.[12–15] The Kirkendall effect, which is a classical phenomenon in metallurgy discovered by Kirkendall a half century ago,[16] was recently applied to design and fabricate hollow spherical nanocrystals.[17–19] The Kirkendall effect was the first experimental evidence that atomic diffusion occurs through vacancy exchange rather than by direct interchange of atoms. This vacancy-assisted transporting mechanism can be considered as the main mode of atomic transport. In this process, the difference in diffusion rates of two interdiffusion species across an interface results in a net directional flow of matter, which is balanced by an opposite flow of vacancies. These vacancies can condense into voids or annihilate at dislocations. This concept has been well demonstrated by Alivisatos and co-workers in recent reports, where hollow cobalt sulfide and gold octahedra have been successfully fabricated.[17,18]

MgO is a typical wide-bandgap insulator, which has drawn special attention due to its important use as a passivation layer in high-electron-mobility transistors,[20] a substrate for thin film growth,[21] and additives in refractory, paint, and superconductor products.[22–24] It has been demonstrated that the incorporation of MgO nanorods into superconductors led to improved performance at an elevated temperature or in intensive magnetic fields,[25] and Ga-filled MgO nanotubes were used as wide-temperature-range nanothermometers.[26] MgO is also widely used as a coating layer, sorbent, catalyst, and catalytic support in catalysis.[27–29] For all these applications, particle size, porosity, and specific surface area are of major importance. The traditional method to prepare MgO is the thermal decomposition of either magnesium salts or magnesium hydroxides, which results in a nonhomogeneity of morphology and crystallite size with a low surface area. Many efforts were therefore exerted to tailor hollow MgO nanostructures with high surface area. However, to the best of our knowledge, only several papers on the synthesis of hollow MgO nanostructures with tubular morphology have been published.

[a] Department of Physics and Key Laboratory of Acoustic and Photonic Materials and Devices, Ministry of Education, Wuhan University,
Wuhan 430072, People's Republic of China
Fax: +86-27-6875-2569
E-mail: jcli@acc-lab.whu.edu.cn
[b] State Key Laboratory of Functional Materials for Informatics, Shanghai Institute of Microsystem and Information Technology, Chinese Academy of Sciences,
865 Changning Road, Shanghai 200050, People's Republic of China

Li et al.[26] prepared Ga-filled MgO nanotubes by means of a liquid-metal-assisted method by using Ga_2O_3 and Mg as the source materials. Zhan et al.[30] obtained tubular MgO nanostructures by heating a mixture of MgO, C, and Ga_2O_3 powders at a high temperature of 1200 °C, where Ga was used as a catalyst in the growth process. Hao et al.[9] fabricated tubular MgO nanostructures by evaporating metal Mg strips at 800 °C. Recently, we also synthesized MgO nanotubes by using a Zn-assisted route by thermal evaporation of the mixed Zn and Mg powders.[10] Therefore, development of a new method to construct MgO nanotubes as well as other novel and complex hollow MgO architectures with desired dimensions and sizes is still highly necessary. In this paper, we report a newly developed solid–gas chemical reaction route to manufacture MgO nanotube arrays by using prefabricated ZnO nanorods as templates. The formation process involves the Kirkendall effect, in which the outdiffusion of the ZnO core material through the MgO shells is faster than the in-diffusion of the vapor-phase Mg atoms, resulting in the formation of Kirkendall voids, which eventually induces hollow MgO nanotubes. The approach presented here is effective and facile without the introduction of additional etching agents, and allows a rational design of hollow structures according to the appropriate choice of starting materials. In light of the fact that the synthetic technology of nanoscale ZnO has been well investigated, and ZnO nanostructures with various crystal size, morphology, and length/width ratio have been successfully synthesized,[3,31–33] various novel and complex hollow MgO architectures with different aspect ratios can therefore be further manipulated and fabricated by this method, depending on the morphologies of ZnO nanostructures used as templates.

Results and Discussion

We first present the morphological and structural changes of the ZnO nanorods before and after reaction with Mg. Figure 1a shows the scanning electron microscopy (SEM) image of the initial ZnO nanorods on Si substrates. The nanorods have an average diameter of about 65 nm and lengths of several micrometers. Homogeneous deposition of these nanorods over areas of several square centimeters is routinely performed. The X-ray diffraction (XRD) pattern (Figure 2a) taken from the initial nanorods displays a strong (002) peak, demonstrating that the nanorods are hexagonal wurtzite ZnO growing along the *c* axis.

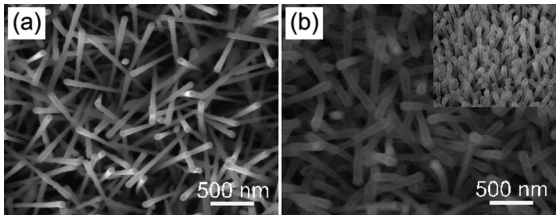

Figure 1. SEM images of (a) the initial ZnO nanorod arrays and (b) MgO nanotube arrays obtained by exposing the ZnO nanorods to Mg vapor at 650 °C for 60 min; the inset shows the side view of the converted MgO nanotube arrays.

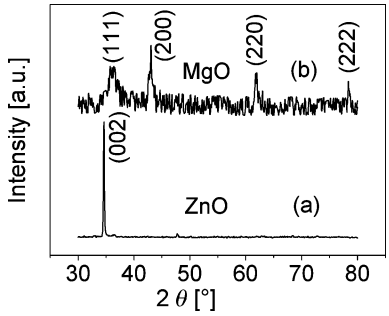

Figure 2. XRD patterns of (a) the initial ZnO nanorods and (b) the converted MgO nanotubes.

Using quasi-aligned ZnO nanorods as templates, we anticipate receiving MgO hollow nanostructures of similar morphology according to the reaction given by Equation (1).

$$ZnO + Mg \rightarrow MgO + Zn \quad (1)$$

Figure 1b shows the SEM image of the converted MgO nanostructures. One may observe that the converted MgO nanostructures seem to have hollow interiors. This will be further confirmed by transmission electron microscopy (TEM) (Figure 3). The side view of the MgO nanotubes is presented in the inset of Figure 1b, showing quasi-aligned MgO nanotubes after the conversion of the ZnO nanorod arrays. These tubes have an average outside diameter of

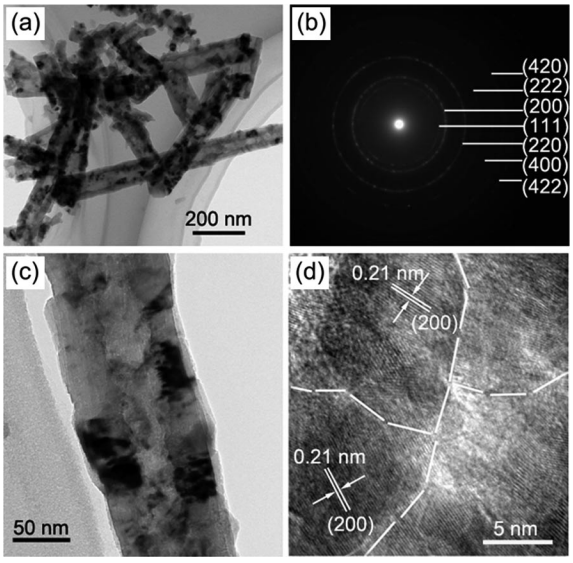

Figure 3. TEM and HRTEM images of MgO nanotubes: (a) typical bright-field TEM images of the MgO nanotubes exhibiting tubular structures; (b) the corresponding SAED pattern of the MgO nanotubes; (c) a typical TEM image of a section of an individual MgO nanotube; (d) the corresponding HRTEM image of the MgO nanotube.

about 102 nm. It is also noted that the surfaces of the nanotubes are quite rough, indicating that the growth process of MgO nanotubes is nonepitaxial, and this finding is also compatible with the idea that the growth of MgO is via a metal ion exchange reaction between Mg and ZnO.

XRD patterns of the initial ZnO nanorods and converted MgO nanotubes are represented in Figure 2a and Figure 2b, respectively. From Figure 2b, one may find that all the peaks can be well-indexed to the cubic MgO with a lattice constant of a = 4.211 Å within experimental error. No other peak is observed in the XRD pattern, revealing that all the ZnO nanorods are transformed completely into cubic MgO structures.

Further insight into the converted MgO nanostructures can be revealed by TEM and high-resolution transmission electron microscopy (HRTEM) images. Figure 3a shows a typical bright-field TEM image of the MgO nanostructures, exhibiting the tubular structure. Owing to the smaller molar volume of MgO relative to ZnO, a slight decrease in the diameter of converted MgO would be expected if solid MgO nanostructures are obtained by conversion of the ZnO nanorods. From the TEM results, however, the converted MgO nanotubes have outside diameters of 90–115 nm, and the majority of them are around 102 nm, which is 157% of that of the starting ZnO nanorods. The increase in diameters of the converted MgO nanotubes is mainly because their hollow structure was caused by the Kirkendall effect (the detailed explanation will be presented later). The inside diameters of the MgO nanotubes range from 30 to 55 nm, with an average diameter of about 40 nm. Figure 3b shows the corresponding selected area electron diffraction (SAED) pattern of the MgO nanotubes. The diffraction rings correspond to the (111), (200), (220), (222), (400), (420), and (422) planes of the cubic MgO. This further confirms that the nanotubes are cubic MgO. Also, in the SAED pattern, besides the diffraction rings corresponding to the cubic MgO structure, no additional ring is clearly observed, which is in coincidence with the results of XRD analysis (Figure 2b). Figure 3c exhibits a typical high-magnification TEM image of a part of an individual MgO nanotube. It is visible that the observed MgO nanostructure is indeed a hollow tubular structure. Careful observations reveal that the tube walls are actually composed of small-sized nanocrystals, whose sizes range from 10 to 35 nm. This can be more clearly observed in the corresponding HRTEM pattern of the nanotube (shown in Figure 3d). Different lattice directive nanocrystals can be clearly seen in the HRTEM image, and part of the boundaries of these nanocrystals are outlined with dashed lines. The measured fringe spacing of 0.21 nm between adjacent lattice planes matches well with the distance of (200) planes of cubic MgO, revealing the single-crystal nature of the nanocrystals.

To further understand the phase and structure transformation from ZnO nanorods to hollow MgO nanotubes, the samples obtained from different conversion stages controlled by reaction time were examined by XRD and TEM. Figure 4 shows XRD patterns of the products obtained at different conversion durations of 20, 40, and 60 min. In the case of the 20 min conversion duration, the XRD pattern (Figure 4a) shows a coexistence of ZnO and MgO phases, indicating that ZnO crystals were partially transformed into cubic MgO. With the increase in reaction time, the relative intensity of ZnO peaks decreases along with the increase in MgO intensity (see Figure 4a and b). When the reaction time was extended to 60 min, only pure cubic MgO structures were obtained according to the XRD (Figure 4c) and SAED (Figure 3b) results. These results reveal that the conversion from ZnO nanorods to MgO nanostructures continues until the depletion of ZnO with increasing reaction time. Therefore, the ratio ZnO/MgO can be easily manipulated by changing the reaction time. Figure 5a and b show bright-field TEM images of the products at different conversion periods (20 and 40 min, respectively). In Figure 5a, ZnO/MgO core/shell nanocables can be clearly identified from the contrast variations between the outer parts and the inner parts, which is consistent with the XRD result (Figure 4a). However, when the conversion process proceeds for 40 min, partially hollow ZnO/MgO nanocables appear. As depicted in Figure 5b, some residual ZnO segments partially fill the cores, resulting in the discontinuous voids in the ZnO/MgO nanocables. Figure 5c presents the TEM image of a partially hollow ZnO/MgO nanocable. The top-right inset in Figure 5c shows the SAED pattern taken from the hollow section of the nanocable (indicated by the circle). Some discontinuous diffraction rings are observed, which can be indexed to cubic

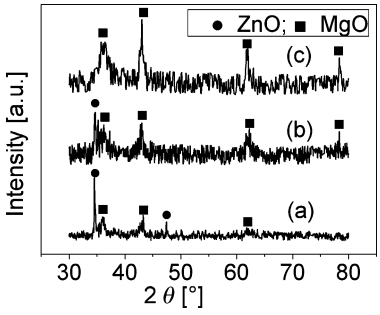

Figure 4. XRD patterns of the products at different conversion periods (conversion from ZnO nanorods to MgO nanotubes): (a) 20 min; (b) 40 min; (c) 60 min.

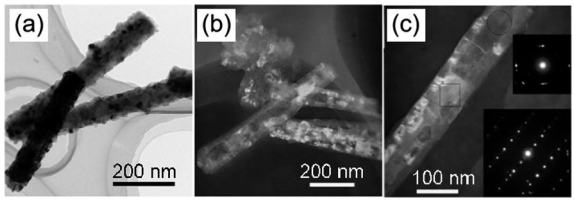

Figure 5. TEM images of the products at different conversion periods: (a) 20 min (showing core/shell nanocable structure); (b) 40 min (partially hollow ZnO/MgO nanocables); (c) the enlarged image of (b), more clearly showing a partially hollow ZnO/MgO nanocable; the top-right and bottom-right insets show the SAED patterns taken from the hollow and solid parts of the nanocable, respectively.

MgO. In contrast, the SAED pattern taken from the solid part of the nanocable (indicated by the rectangle) and displayed in the bottom-right of Figure 5c contains a spotted diffraction pattern of wurtzite ZnO taken along the $[2\bar{1}\bar{1}0]$ zone axis, which comes from the single-crystalline ZnO core, and some weak diffraction spots correspond to cubic MgO. The partially hollow structure of ZnO/MgO nanocables implies that the conversion reaction between ZnO and Mg occurs through the outer MgO shells.

On the basis of the above results and the analysis of the morphologic and structural characterizations of the samples obtained at different conversion durations, a formation process involving the core/shell structural ZnO/MgO nanocables, partially hollow ZnO/MgO nanocables, and completely hollow MgO nanotubes can be deduced. It is surprising that solid ZnO nanorods could change into hollow MgO nanotubes by a substitution reaction between Mg and ZnO. In the previous reports, ZnO nanorods were also used as templates to fabricate ZnS nanotubes, where ZnS nanotubes were obtained by the removal of ZnO cores of ZnO/ZnS nanocables by KOH treatment.[35] MgO nanotubes were also produced at 650 °C by the sublimation of Zn cores from Zn/MgO core/shell configurations[10] by taking advantage of the low melting point of the Zn core (around 419 °C). In our present case, since the ZnO core has a high melting point (around 1975 °C) and no additional solvent was introduced, the formation mechanism of our MgO nanotubes is obviously different from those reported previously, but is attributed to the Kirkendall effect. In our present system, ZnO and vapor-phase Mg atoms can react with each other and form a diffusion pair. The coupled reaction/diffusion at the solid–gas interface could lead to the quick formation of an interconnected MgO shell around the external surface of the ZnO nanorods (see Figure 5a). The outer MgO shell prevents a direct chemical reaction, and further reaction relies on the diffusion of ZnO and Mg through the shell. Because O ions in ZnO diffuse faster than Mg atoms, a net outward flow of O ions through the MgO shell results in the opposite transport of lattice vacancies. These vacancies would condense to form voids in ZnO cores, causing the partially hollow morphology of the ZnO/MgO nanocables (shown in Figure 5b), which eventually results in hollow MgO nanotubes after prolonged reaction times (see Figure 3a). A mechanism similar to this one has been demonstrated in the formation of CoO, CoSe, and Au hollow nanocrystals.[17,18] Structurally, MgO has a cubic structure with a = 4.211 Å and ZnO has a hexagonal crystal structure with lattice constants a = 3.249 Å and c = 5.206 Å. During the growth of MgO nanotubes, the oxygen atoms rearrange themselves from a wurtzite to a cubic lattice structure, thus grains or nanocrystallites can be formed. As can be seen in Figure 3d, nanocrystallite boundaries in the tube walls of MgO are clearly observed. It should also be noted that the average inside diameter of MgO nanotubes is about 41 nm, which is approximately 63% of the average diameter (about 65 nm) of the starting ZnO nanorods. If we assume that Mg transport through the MgO shells is negligible, then the two diameters would be expected to be equal. The reduced diameter of the hollow sections indicates the inward diffusion of part of the Mg atoms through the MgO shells, which can occur during the initial stage of the formation of MgO. Meanwhile, the diffusion rate of Mg atoms along grain boundaries should be high, because the nanocrystallite grain boundaries within the MgO shells provide a fast diffusing channel for the inward diffusion of Mg atoms.

Temperature was found to be an important factor in the formation of hollow MgO nanostructures in our method. At low reaction temperature, the reaction rate and the reactant diffusion decrease observably, which lead to the formation of ZnO/MgO core/shell nanocables (not shown here). Our synthetic strategy here also allows further manipulation of the hollow structures of MgO. In addition to the thin MgO nanotubes, larger MgO nanotubes can also be effectively obtained by using thick ZnO nanorod array templates, as shown in Figure 6a. The outside diameters of the MgO nanotubes and starting ZnO nanorods are 250–300 nm and 180–200 nm, respectively. The inside diameters of the MgO nanotubes range from 110 to 150 nm. So the dimensions and diameters of the MgO nanotubes can be controlled easily by employing suitable ZnO templates. We also used comb-like ZnO nanostructures as starting material and obtained comb-like MgO nanostructures consisting of tubular stems and hollow teeth (shown in Figure 6b) at a conversion temperature of 650 °C. Other types of novel and complex hollow MgO architectures can be further tailored and fabricated by this method, depending on the morphologies of the starting ZnO nanostructures used as templates. These complex MgO hollow architectures might find potential in highly integrated multichannel applications.

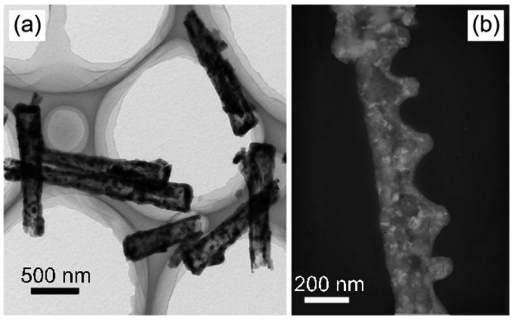

Figure 6. (a) TEM image of MgO nanotubes with large diameters obtained by using thick ZnO nanorods as templates; (b) TEM image of a typical two-dimensional comb-like MgO nanotube synthesized by using comb-like ZnO nanostructure as a starting template.

Optical investigations can reveal very useful information for understanding the physical properties of materials. They also demonstrate the possibility to extend the potential application of MgO nanostructures in optoelectronic devices. Figure 7 shows the room-temperature photoluminescence (PL) spectra of the initial ZnO nanorods as well as the converted ZnO/MgO nanocables and MgO nanotubes. The ZnO/MgO nanocables and MgO nanotubes here were obtained by exposing the initial ZnO nanorods to Mg vapor

at 650 °C for 20 and 60 min, respectively. As shown in Figure 7a, the initial ZnO nanorod arrays show a UV emission at 381 nm, which originates from the excitonic recombination corresponding to the band-edge emission of ZnO.[36] The converted MgO nanotubes exhibit a different emission band from that of the ZnO nanorod templates, centered at about 393 nm (shown in Figure 7c). Rosenblatt et al.[37] have reported the 390 and 530 nm bands in time-resolved spectra of bulk MgO with different defect densities, and attributed the bands to F^+ and F centers, respectively. In our experiment, rapid evaporation, incomplete crystallization, and formation of the polycrystalline phase may induce various structural defects, such as different kinds of oxygen vacancies, etc. In addition, the high-surface-to-volume-ratio MgO nanotubes composed of small nanocrystals should also favor the existence of large quantities of structural defects. These structural defects would induce the formation of new energy levels in the bandgap of the MgO, contributing to the observed 393 nm emission band of the MgO nanotubes. In the PL spectrum of the ZnO/MgO nanocables, two shoulder emissions centered at about 381 nm and 393 nm are observed (shown in Figure 7b). It is evident that the ZnO/MgO nanocables hold the PL properties of both ZnO and MgO. The emission at 381 nm corresponds to the near-band-edge peak of the ZnO cores, and the emission located at 393 nm results from the MgO shells. Further research indicates that the ratio of ZnO/MgO nanocables has great effects on the relative intensity and peak position of typical PL emission of ZnO/MgO nanocable arrays. So the properties of these nanostructures can be modulated simply by changing their structures through the control of reaction time.

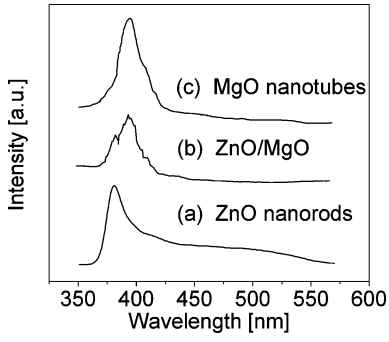

Figure 7. Room-temperature PL spectra of (a) the initial ZnO nanorods; (b) the ZnO/MgO nanocables; (c) the converted MgO nanotubes.

Conclusions

In summary, we have demonstrated an effective and versatile route to the synthesis of hollow MgO nanotube arrays by the reaction of ZnO nanorods with Mg vapor. The dimensions of the obtained MgO nanotubes, including diameters and wall thicknesses, can be controlled by varying the starting ZnO templates. Other novel and complex hollow MgO architectures with different aspect ratios can be also manipulated and fabricated by this method, depending on the morphologies of the ZnO nanostructures used as templates. The convenient control of the conversion ratio of ZnO/MgO by the reaction time can therefore enable the properties of these composite materials to be moderately modulated. These hollow MgO nanostructures with high surface-to-volume ratios may find potential applications in catalysis, drug delivery, nanoreactors, and active material encapsulation. Furthermore, the current work provides a general route to the synthesis of hollow MgO architectures. It can also be extended to the manufacture of other oxides with hollow structures.

Experimental Section

ZnO nanorods were synthesized on Si(100) substrates by a thermal evaporation technology of metallic Zn powder. Zinc powder (99.9% in purity) was placed on a quartz boat that was inserted into the center of a horizontal tube furnace. Cleaned Si substrates were located at about 8 mm downstream from the Zn source. The system was first pumped to a base vapor pressure of about 5 Pa, and then argon [70 sccm (standard cubic centimeter per minute)] and air (80 sccm) were introduced into the system. Afterwards, the tube was heated to 460 °C at a rate of 25 °C/min. The synthesis process was carried out under a pressure of 20 Pa at 460 °C and lasted for about 60 min. The gas flows were cut off when the power of furnace was turned off, and the samples were then naturally cooled to 5 Pa. In this case, ZnO nanorods with an average diameter of about 65 nm were obtained. By simply varying the preparation parameters, including growth temperature, distances between substrates and Zn powder, gas flow rate, and the starting time of air introduction, ZnO nanorods with different diameters, ZnO nanobelts, microspheres, and other nanostructures can be synthesized.[3,11,34]

The as-synthesized ZnO nanostructures were then used as templates for the fabrication of MgO nanostructures. We placed the substrates covered with as-synthesized ZnO templates together with Mg powder (1 g) on a quartz boat, and inserted the quartz boat into the center of a horizontal tube furnace. The distance between substrates and the Mg source was about 1 cm. The furnace chamber was first pumped to a base vapor pressure of about 5 Pa under a constant flow of high-purity Ar (70 sccm). Afterwards, the furnace was rapidly heated to 650 °C and the temperature was maintained for 1 h. The furnace was then cooled down slowly.

The morphology and crystalline structure of the converted samples were characterized by Sirion FEG SEM, D8 advanced XRD, JEOL JEM 2010 TEM and HRTEM. The room-temperature PL spectra were measured by using a He–Cd laser as excitation source (325 nm).

Acknowledgments

This work was supported by the National Natural Science Foundation of China (Grant No. 10575078).

[1] Y. Liu, Y. Chu, L. L. Li, L. H. Dong, Y. J. Zhuo, *Chem. Eur. J.* **2007**, *13*, 6667–6673.
[2] S. Stankic, M. Müller, O. Diwald, M. Sterrer, E. Knozinger, J. Bernardi, *Angew. Chem. Int. Ed.* **2005**, *44*, 4917–4920.
[3] L. Liao, H. B. Lu, J. C. Li, H. He, D. F. Wang, D. J. Fu, C. Liu, W. F. Zhang, *J. Phys. Chem. C* **2007**, *111*, 1900–1903.

[4] F. Caruso, *Chem. Eur. J.* **2000**, *6*, 413–419.
[5] S. M. Marinakos, M. F. Anderson, J. A. Ryan, L. D. Martin, D. L. Feldheim, *J. Phys. Chem. B* **2001**, *105*, 8872–8876.
[6] M. Remškar, A. Mrzel, M. Viršek, A. Jesih, *Adv. Mater.* **2007**, *19*, 4276–4278.
[7] M. M. Titirici, M. Antonietti, A. Thomas, *Chem. Mater.* **2006**, *18*, 3808–3812.
[8] B. Putlitz, K. Landfester, H. Fischer, M. Antonietti, *Adv. Mater.* **2001**, *13*, 500–503.
[9] Y. F. Hao, G. W. Meng, Y. Zhou, M. G. Kong, Q. Wei, M. Ye, L. D. Zhang, *Nanotechnology* **2006**, *17*, 5006–5012.
[10] H. B. Lu, L. Liao, H. Li, Y. Tian, J. C. Li, D. F. Wang, B. P. Zhu, *J. Phys. Chem. C* **2007**, *111*, 10273–10277.
[11] H. B. Lu, L. Liao, J. C. Li, D. F. Wang, H. He, Q. Fu, L. Xu, Y. Tian, *J. Phys. Chem. B* **2006**, *110*, 23211–23214.
[12] Z. Zhong, Y. Yin, B. Gates, Y. Xia, *Adv. Mater.* **2000**, *12*, 206–209.
[13] F. Caruso, X. Shi, R. A. Caruso, A. Susha, *Adv. Mater.* **2001**, *13*, 740–744.
[14] M. C. Neves, T. Trindade, A. M. B. Timmons, J. D. Pedrosa de Jesus, *Mater. Res. Bull.* **2001**, *36*, 1099–1108.
[15] F. Caruso, R. A. Caruso, H. Mohwald, *Science* **1998**, *282*, 1111–1114.
[16] A. D. Smigelskas, E. O. Kirkendall, *Trans. Am. Inst. Min. Metall. Eng.* **1947**, *171*, 130.
[17] Y. D. Yin, R. M. Rioux, C. K. Erdonmez, S. Hughes, G. A. Somorjai, A. P. Alivisatos, *Science* **2004**, *304*, 711–714.
[18] Y. D. Yin, C. Erdonmez, S. Aloni, A. P. Alivisatos, *J. Am. Chem. Soc.* **2006**, *128*, 12671–12673.
[19] K. N. Tu, U. Gosele, *Appl. Phys. Lett.* **2005**, *86*, 093111.
[20] B. Luo, J. W. Johnson, J. Kim, R. M. Mehandru, F. Ren, B. P. Gila, A. H. Onstine, C. R. Abernathy, S. J. Pearton, A. G. Baca, R. D. Briggs, R. J. Shul, C. Monier, J. Han, *Appl. Phys. Lett.* **2002**, *80*, 1661–1663.
[21] J. C. Jiang, E. I. Meletis, Z. Yuan, C. L. Chen, *Appl. Phys. Lett.* **2007**, *90*, 051904.
[22] A. Bhargava, J. A. Alarco, I. D. R. Mackinnon, D. Page, A. Iiyushechkin, *Mater. Lett.* **1998**, *34*, 133–142.
[23] Y. S. Yuan, M. S. Wong, S. S. Wang, *J. Mater. Res.* **1996**, *11*, 8–17.
[24] G. W. Wagner, P. W. Bartram, O. Kopper, K. J. Klabunde, *J. Phys. Chem. B* **1999**, *103*, 3225–3228.
[25] P. D. Yang, C. M. Lieber, *Science* **1996**, *273*, 1836–1840.
[26] Y. B. Li, Y. Bando, D. Golberg, Z. W. Liu, *Appl. Phys. Lett.* **2003**, *83*, 999–1001.
[27] H. S. Jung, J. K. Lee, M. Nastasi, S. W. Lee, J. Y. Kim, J. S. Park, K. S. Hong, H. Shin, *Langmuir* **2005**, *21*, 10332–10335.
[28] G. Pacchioni, T. Minerva, R. S. Bagus, *Surf. Sci.* **1992**, *275*, 450–458.
[29] H. Itoh, S. Utamapanya, J. V. Stark, K. J. Klabunde, J. R. Schlup, *Chem. Mater.* **1993**, *5*, 71–77.
[30] J. H. Zhan, Y. S. Bando, J. Q. Hu, D. Golberg, *Inorg. Chem.* **2004**, *43*, 2462–2464.
[31] B. Q. Cao, X. M. Teng, S. H. Heo, Y. Li, S. O. Cho, G. H. Li, W. P. Cai, *J. Phys. Chem. C* **2007**, *111*, 2470–2476.
[32] Q. X. Zhang, K. Yu, W. Bai, Q. Y. Wang, F. Xu, Z. Q. Zhu, N. Dai, Y. Sun, *Mater. Lett.* **2007**, *61*, 3890–3892.
[33] Z. R. R. Tian, J. A. Voigt, J. Liu, B. McKenzie, M. J. McDermott, M. A. Rodriguez, H. Konishi, H. F. Xu, *Nat. Mater.* **2003**, *2*, 821–826.
[34] L. Liao, J. C. Li, D. H. Liu, C. Liu, D. F. Wang, W. Z. Song, Q. Fu, *Appl. Phys. Lett.* **2005**, *86*, 083106.
[35] C. L. Yan, D. F. Xue, *J. Phys. Chem. B* **2006**, *110*, 25850–25855.
[36] Y. C. Kong, D. P. Yu, B. Zhang, W. Fang, S. Q. Feng, *Appl. Phys. Lett.* **2001**, *78*, 407–409.
[37] G. H. Rosenblatt, M. W. Rowe, G. P. Williams Jr, R. T. Williams, Y. Chen, *Phys. Rev. B* **1989**, *39*, 10309–10318.

Received: January 25, 2008
Published Online: May 6, 2008

